(Received 1 December 2025, Accepted 31 December 2025, Scheduled 18 January 2026)

Optimized NCP MIMO Antenna with Dual Diamond Slots for Enhanced Isolation in 5G Applications

Rama Lakshmi Gali[1, 2, *] and Madhavi Tatineni[1]

[1] Department of EECE, GITAM School of Technology, Hyderabad, India
[2] Department of ECE, BVRIT Hyderabad College of Engineering for Women, Hyderabad, India

ABSTRACT: This research paper presents a novel two-element Notched Circular Patch (NCP) antenna tailored for n78 5G NR band communication, resonating at a frequency of 3.5 GHz. The primary focus of this study is to enhance isolation using a simple antenna design with advanced optimization techniques. The proposed NCP antenna incorporates two diamond-shaped slots within a circular patch, designed to operate at n78 band or C-band. Through meticulous design and fabrication processes, the antenna achieves an inter-element spacing that is optimized with GA algorithm, and 1/4 of the ground structure is considered at the center of the patch, significantly improving its performance at 3.5 GHz and maintaining a VSWR of 1.1. The proposed $60 \times 30\,\text{mm}^2$ NCP antenna exhibits remarkable characteristics, including > -30 dB isolation, a reflection coefficient of -27 dB, and a gain of 4 dBi. These results underscore the effectiveness of the antenna design in reducing mutual coupling and enhancing isolation, which are essential for achieving reliable and efficient communication in 5G. The NCP MIMO antenna is thoroughly analyzed using characteristic mode analysis (CMA), and CMA parameters' influence on antenna performance is discussed. The design further highlights its practicality and potential for implementation in various wireless communication systems.

1. INTRODUCTION

In the future, all systems will work with advanced wireless communication, and for better coverage, multiple-input multiple-output (MIMO) antennas will be used in communications [1]. They boost signal potency within an established radio link and have been incorporated into modern wireless standards, such as WLAN, LTE, and 5G [2, 3]. These standards are in a new era of enhanced system capacity and user scalability, boasting elevated data rates while mitigating signal fading through the incorporation of diverse methods and deployment of multiple antennas. The strides made recently owe much to the diligent efforts of antenna designers who have significantly advanced the development of planar MIMO antennas.

In the quest for innovation, myriad design techniques have been employed, resulting in the profusion of advanced antenna structures [4]. These innovations, which are driven by the need to meet evolving performance requirements, include a broad spectrum of methodologies. One notable approach is decoupling method, which seeks to reduce mutual coupling between closely placed antenna elements. This technique enhances the overall performance and efficiency of multi-element antenna systems, making it a cornerstone in the development of modern communication systems. Another significant breakthrough is the use of parasitic elements, which are passive components strategically placed near active radiating elements. These parasitic elements manipulate the electromagnetic field distribution to improve parameters such as gain, bandwidth, and directivity. This concept has been widely adopted in the design of directional antennas, including Yagi-Uda arrays.

The exploitation of degenerated resonant modes represents an advanced antenna design strategy that enables precise control over radiation characteristics, such as impedance bandwidth and polarization behavior. By selectively exciting specific modes of the antenna structure, this technique offers enhanced performance flexibility, particularly in compact designs, where physical constraints limit conventional optimization approaches [5]. Neutralization line techniques have also emerged as effective solutions for mitigating mutual coupling in multi-input multi-output antenna systems. The introduction of neutralization lines counteracts the coupling currents between adjacent radiating elements, thereby improving port isolation, enhancing signal integrity, and reducing interference in high-density communication environments [5]. Another significant advancement is the development of dual-band antenna arrays that are capable of operating efficiently over two distinct frequency bands. Such designs are particularly relevant for modern wireless applications, including 5G systems, where efficient spectrum utilization across multiple bands is essential [6]. Furthermore, hybrid design approaches that combine multiple decoupling and feeding techniques have been investigated to minimize insertion loss and optimize the overall antenna performance [7]. For example, the use of multiple feedlines in conjunction with diagonally placed parasitic elements provides balanced excitation and improve radiation efficiency [8]. In addition, advanced decoupling methods for antenna arrays play a critical role in suppressing the mutual coupling effects, particularly in large-scale MIMO configu-

* Corresponding author: Rama Lakshmi Gali (ramalakshmi.gali@gmail.com).

rations [9, 15]. Innovative substrate-based solutions, such as the quarter-mode substrate integrated waveguide (QMSIW), have further broadened the scope of compact antenna design. QMSIW structures enable high-performance operation while significantly reducing the substrate size and material usage, thereby achieving compactness without sacrificing electromagnetic performance [10].

The use of interconnected ground for symmetric patterns provides a robust framework for achieving stable and consistent radiation patterns. This technique is particularly beneficial in applications that require symmetrical coverage [11–13]. Ground modifications, such as defected ground structure-based antennas, ground-printed antennas, and double-sided MIMO antennas, have also gained prominence. Defected ground structures introduce intentional disruptions in the ground plane to enhance the bandwidth and reduce the size, whereas ground-printed designs leverage ground layers for additional functionality.

Finally, the development of double-sided MIMO antennas featuring symmetrical circular elements and asymmetrical coplanar strip wall loadings exemplifies the cutting edge of antenna design [14, 15]. These designs ensure optimized isolation, enhanced gain, and improved bandwidth, paving the way for high-performance, compact communication systems. Altogether, these innovations highlight the relentless drive toward refining antenna technologies to meet the ever-growing demands of modern wireless communication systems. Each technique contributes uniquely, ensuring that antenna designs remain at the forefront of technological progress. This represents only a fraction of the diverse designs available for 5G communication MIMO antennas. Some of these antennas leverage two elements [16–19], four elements [20–22], or arrays of elements to achieve optimal isolation, marking a significant leap forward in the quest for efficient and reliable 5G communication [23–25].

Despite significant progress, mutual coupling and signal interference between the antenna elements remain persistent issues in compact MIMO systems. These problems are particularly pronounced in space-constrained environments in which the antennas are positioned in proximity. Additionally, maintaining high isolation without resorting to complex or bulky structures continues to be a challenge for antenna designers. The growing need for dual-band operation across critical frequencies, such as 3.3–4.2 GHz spectrum used in 5G-NR N78 and C-band communications, adds another layer of design complexity.

This study introduces a novel design featuring a printed circular patch with two suspended diamond slots, an inter-element spacing between the patches of 6 mm, and a ground reduction approach to enhance isolation and reduce mutual coupling. Employing two elements, this design forms a circular-polarized MIMO antenna with interelement spacing, slotted patch, hatched ground, and compact size to boost the overall antenna performance. The results of the simulations and measurements demonstrate the superior performance of the proposed antenna.

2. DESIGN OF PATCH ANTENNA

2.1. Single Patch Antenna

A microstrip antenna consists of a radiating patch on one end of a dielectric substrate and a ground plane on the other end can have any shape. One of the most common dielectric materials used in patch antennas is FR-4, making it an affordable choice for various RF applications; however, it has some limitations in terms of losses at high frequencies.

The design started with an analytical formulation based on the standard equations of the resonant behavior of circular patch antennas. The effective radius of the patch element at the target resonant frequency was calculated using these expressions. The radius of the patch considered circular is computed based on the following relationship:

$$d = \frac{P}{\left\{1 + \frac{2h}{\pi\varepsilon_r P}\left[\ln\left(\frac{\pi P}{2h}\right) + 1.7726\right]\right\}^{\frac{1}{2}}} \tag{1}$$

$$P = \frac{8.791 \times 10^9}{f_r\sqrt{\varepsilon_r}} \tag{2}$$

Designing an innovative antenna requires a systematic approach that combines theoretical foundations, simulation tools, prototyping, and validation. The substrate used for the simulation is FR-4 with a thickness of 1.6 mm and a dimension substrate length of 34 mm, and width of 30 mm. The FR-4 material used in the design has a dielectric constant of 4.3 and a tangent loss of 0.025. The design process began with a single antenna element featuring a circular patch, followed by circular cuts and a rectangular bar with diamond slots suspended within the circular cut structures. The introduction of circular slots perturbs the surface current paths on the circular patch by increasing the effective electrical length, without increasing the physical size. These slots force the surface currents to flow around the slot edges, resulting in current concentration along the end and center of the diamond boundaries. This redistribution generates additional resonant modes and improves the impedance matching by introducing capacitive loading, thereby enabling the antenna to operate effectively within the desired frequency band. Ground slicing modifies the current flow on a common ground plane by introducing discontinuities. These discontinuities suppress surface-wave propagation and reduce near-field coupling between adjacent antenna elements. As a result, the mutual coupling currents induced in the neighboring elements are significantly attenuated, leading to improved isolation without compromising the radiation efficiency. These structural modifications are aimed at achieving the required resonant frequency for the proposed structure, which is suitable for applications in the lower sub-6 GHz region. The antenna underwent iterative adjustments at different stages to optimize its performance. Figure 1 shows a five-stage model for effective and innovative antenna design. A basic circular-shaped patch is considered to start the process in stage-1 (AS_1).

AS_2, the next stage, is simplified with a reduced patch structure with a circular cut near the feed line to enhance the properties of the antenna. The later stage AS_3 is placed with

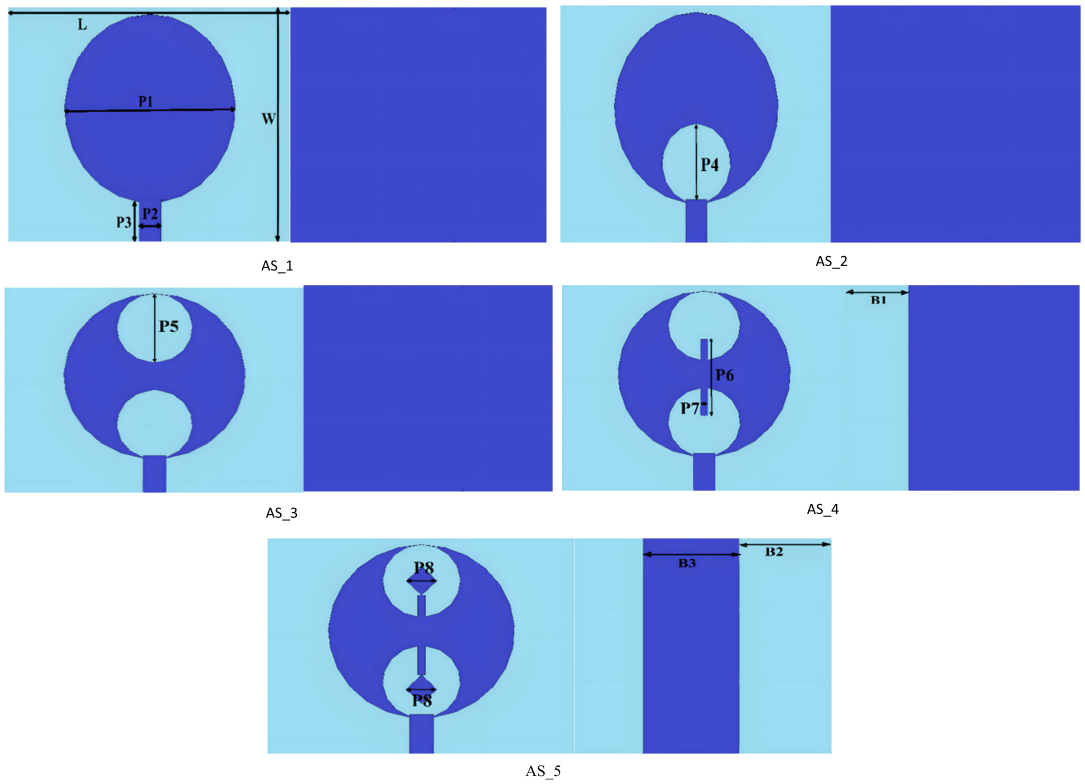

FIGURE 1. Single patch antenna AS_1 to AS_5 stages and its geometry front and back view.

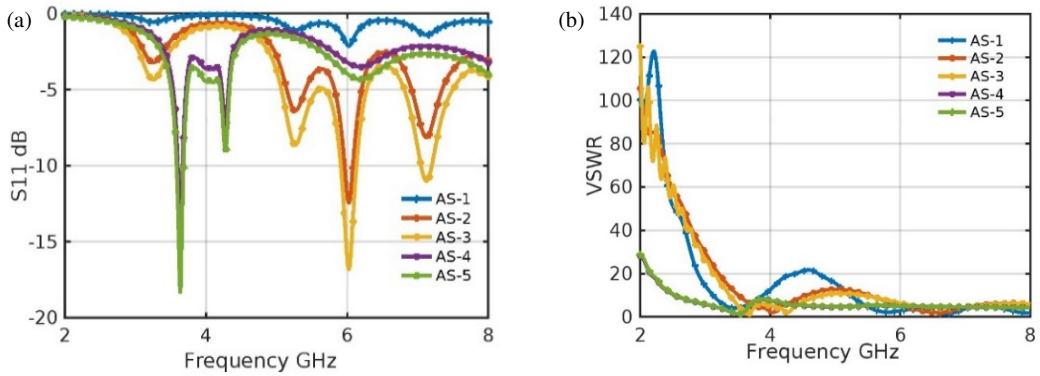

FIGURE 2. (a) S_{11} plot for AS_1 to AS_5. (b) VSWR for AS_1 to AS_5.

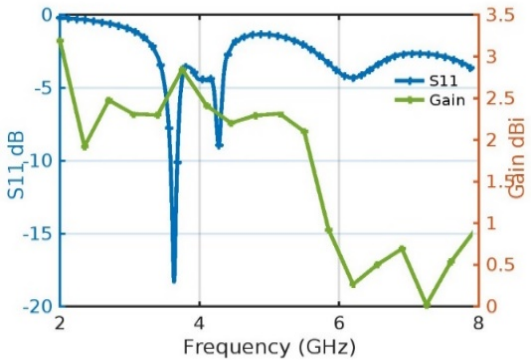

FIGURE 3. AS_5 S_{11} and gain vs frequency parameter values.

another circular cut at the top to balance the impedance of the patch. In the first three stages, the ground is uniform, and the next two stages are vertically sliced to improve radiation properties. In the next stage, AS_4, a small vertical slot is added to match the flow of charge inside the patch. In AS_5, diamond slots are attached to enhance the gain of the antenna. In this stage, the antenna resonates at 3.5 GHz frequency and satisfies the design parameters.

The complete analysis at each stage is recorded and compared with the later stages. The S_{11} values of all five stages are shown in Figure 2(a) with -18 dB. voltage standing wave ratio (VSWR) is plotted in Figure 2(b) with 1.4 for AS_5. Subsequently, the simulated results of a single patch antenna are compared with those of the fabricated model. Figure 3 shows

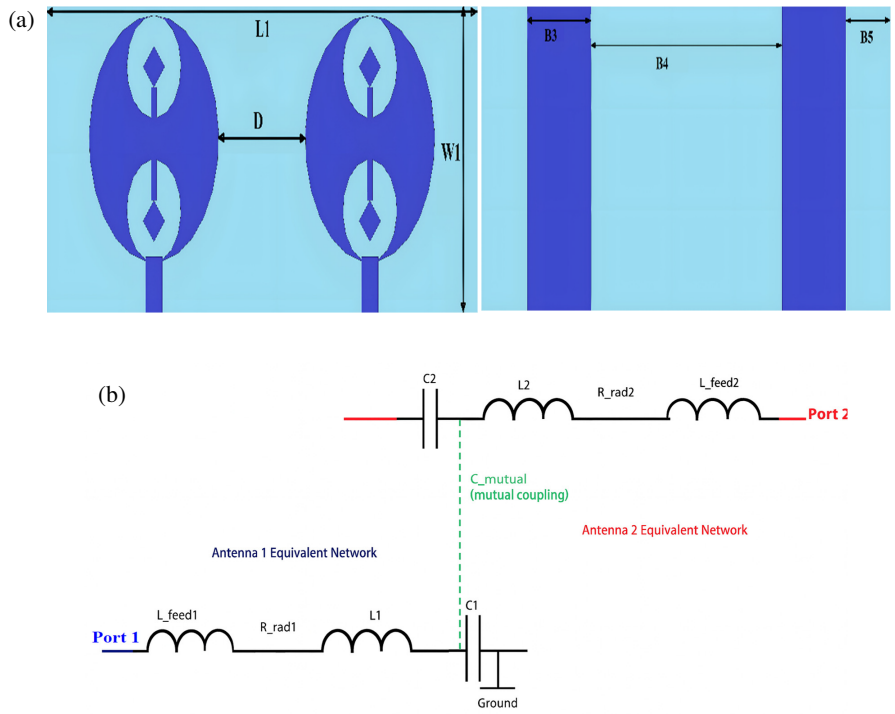

FIGURE 4. (a) Structure of front and back notched circular patch simulated design. (b) Equivalent circuit for the NCP-designed antenna.

the plot of the AS_5 gain and S_{11} vs. frequency. The gain for single-stage AS_5 is 2.7 dBi.

2.2. MIMO NCP Antenna

A design analysis was employed in the development of a MIMO antenna tailored for sub-6-GHz applications in 5G wired scenarios. The performance of a single antenna can be further improved using the concept of MIMO [21]. The MIMO antenna designed with identical patches is placed on the substrate using the inter-element spacing method to ensure that the radiation on one patch will not influence the other, as shown in Figure 4(a) and the equivalent diagram in Figure 4(b). The suggested approach involves determining the inter-element spacing between patches and reducing the mutual coupling between the MIMO antenna systems [2, 5, 22] with optimization algorithms.

Here is a generic algorithm for optimizing the inter-element distance (D) between elements in the proposed MIMO antenna array (as shown in the design) using a Genetic Algorithm (GA) approach. This algorithm is tailored for maximizing performance metrics such as isolation, bandwidth, or minimizing mutual coupling.

1. Encoding: Represent each potential solution as a chromosome where each gene encodes the distance D between adjacent antenna elements.

2. Initialization: Generate an initial population of N chromosomes with randomly selected values for D, within physical and electrical design limits ($D_{\min}$ to $D_{\max}$).

3. Fitness Evaluation: For each chromosome, simulate the MIMO antenna array with the given distance D. Performance metrics, such as $|S_{21}|$, isolation, bandwidth, and envelope correlation coefficient, are calculated to fitness score based on desired criteria.

4. Selection: Use the selection method to choose chromosomes for reproduction, favouring higher fitness scores.

5. Crossover: Randomly select pairs of parent chromosomes and perform crossover to create offspring with mixed genes (distances D).

6. Mutation: With a small probability, mutate genes (D values) in offspring to introduce genetic diversity by randomly changing D within allowed limits.

7. Replacement: Form a new generation by replacing the least-fit individuals with new offspring.

8. Iteration: Repeat steps 3–7 for a set number of generations or until the convergence/stopping criterion is met.

9. Result Extraction: Select the chromosome with the highest fitness as the optimized element spacing D for the MIMO antenna.

The optimized dimensions of the NPC antenna are a length of 60 mm and a width of 30 mm using the GA. The dimensions of the designed stages of the antennas are listed in Table 1.

In designing the MIMO structure, the distance between the patches is a more important factor. If the distance is not optimized properly, insertion losses will be added and affect antenna performance. To optimize the distance, various analyses are performed by placing the antenna at different locations, starting from 9 mm to 5 mm. S_{11} is $-4.6, 13.3, -20.6, -27.04$, and -0.59 for the inter-element distance 9 mm, 8 mm, 7 mm, 6 mm, 5 mm, respectively. S_{21} is below -30 dB with all distances. After careful analysis of the S_{11} and S_{21} parameters at each distance, the distance is confined with the best return loss, and low mutual coupling is at 6 mm. The 6 mm spacing is not selected purely through empirical optimization. This

TABLE 1. Dimension of the single stage and NCP patch designed.

Parameter	L	W	P1	P2	P3	P4	P5	P6	P7
Dimension (mm)	36	30	24	3	5	10	10	12	1
Parameter	P8	B1	B2	B3	L1	W1	D	B4	B5
Dimension (mm)	4	13	13	10	60	30	6	20	10

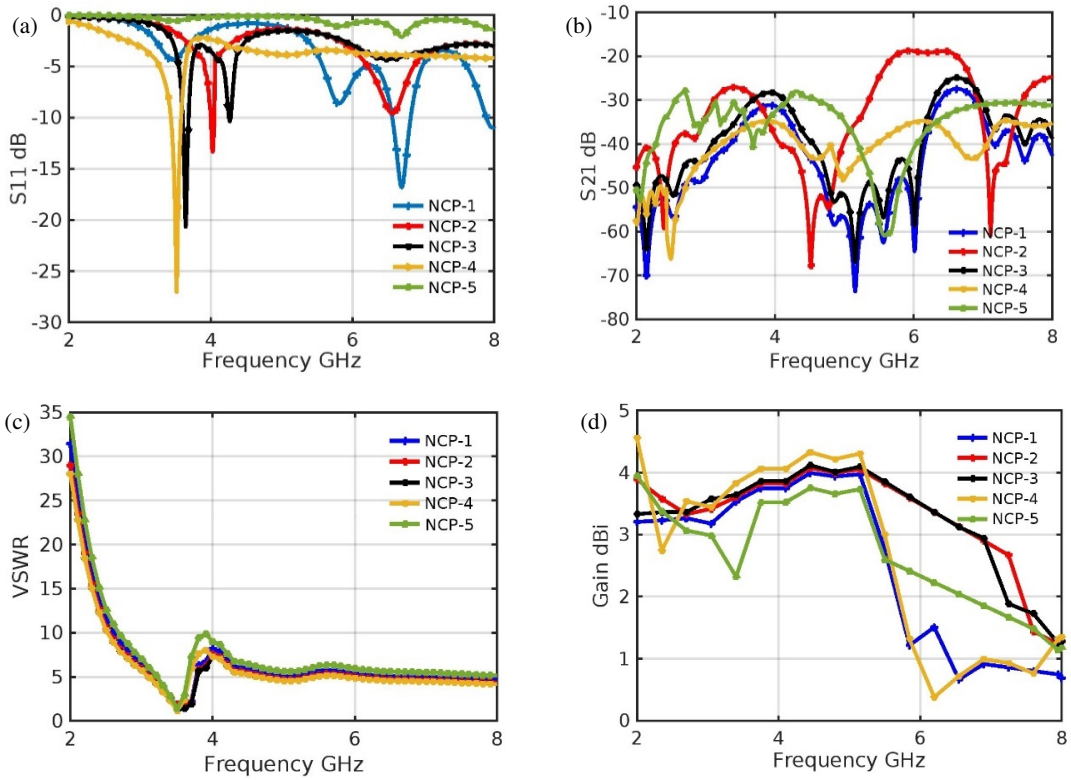

FIGURE 5. (a) S_{11} of NCP at all stages. (b) S_{21} of NCP at all stages. (c) VSWR of NCP at all stages. (d) Gain for all stages.

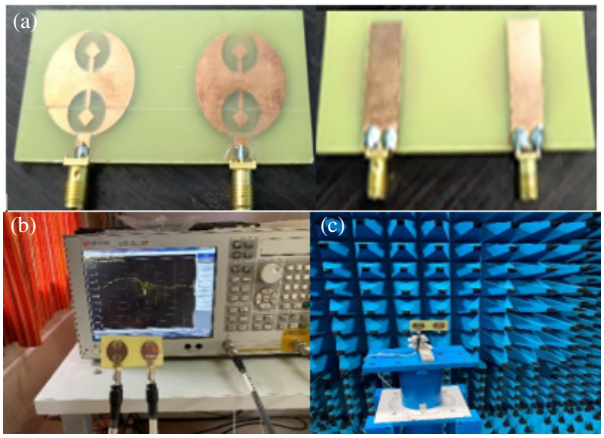

FIGURE 6. (a) NCP-4 fabricated front and back views, (b) testing using VNA, and (c) anechoic chamber.

corresponds to a sub-wavelength separation of nearly 0.07λ at 3.5 GHz, where a balance is achieved between compactness and electromagnetic decoupling. Parametric analysis shows that spacings below 6 mm resulted in strong near-field coupling dominated by electric fields, degrading isolation, and envelope correlation coefficient (ECC).

In this section, the NCP antenna with varying distances between the patch's performances is presented. The distances between patches 9, 8, 7, 6, and 5 mm are used to evaluate the S_{11} and S_{21} parameters for NCP-1, NCP-2, NCP-3, NCP-4, and NCP-5, respectively. Figure 5(a) shows the S_{11} characteristics at these distances. From Figure 5, when the distance between the two elements is 9 mm, the return loss is -4.6 dB. In the next stage (8 mm), the return loss is a bit improved, but resonates at 4 GHz with 13.3 dB. In the 7 mm distance, the resonance shifted to 3.64 GHz with 20.6 dB. At a distance of 6 mm, S_{11} is 27 dB, with a bandwidth of 140 MHz. After this distance is further decreased to 5 mm, the interference is greater, and the radiation of the antenna deteriorates. S_{21} also suggests better values for a distance of 6 mm, as shown in Figure 5(b). Figure 5(c) shows VSWR of all stages, NCP-4 has better VSWR values of 1.16, and Figure 5(d) shows the gain for all stages with 3.6, 3.7, 3.72, 4, and 3.2, respectively.

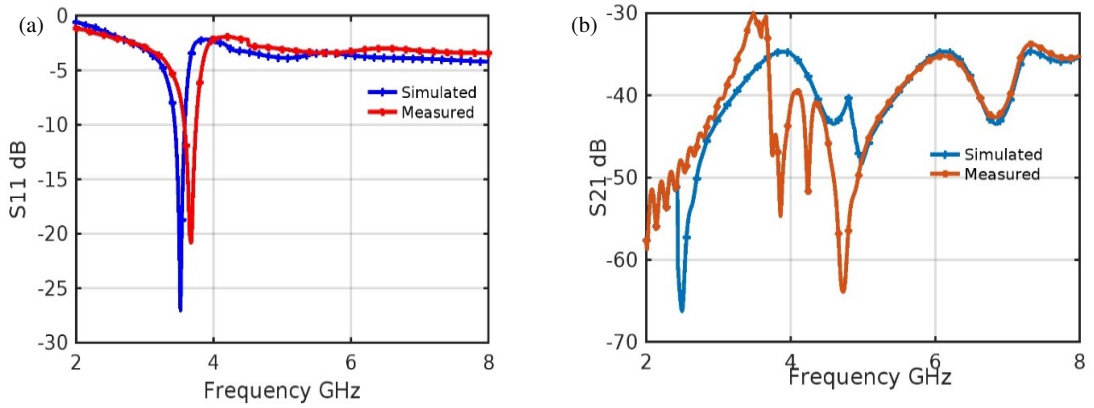

FIGURE 7. (a) S_{11} simulation vs measurement of NCP-4 antenna. (b) S_{21} simulation vs measurement of NCP-4 antenna.

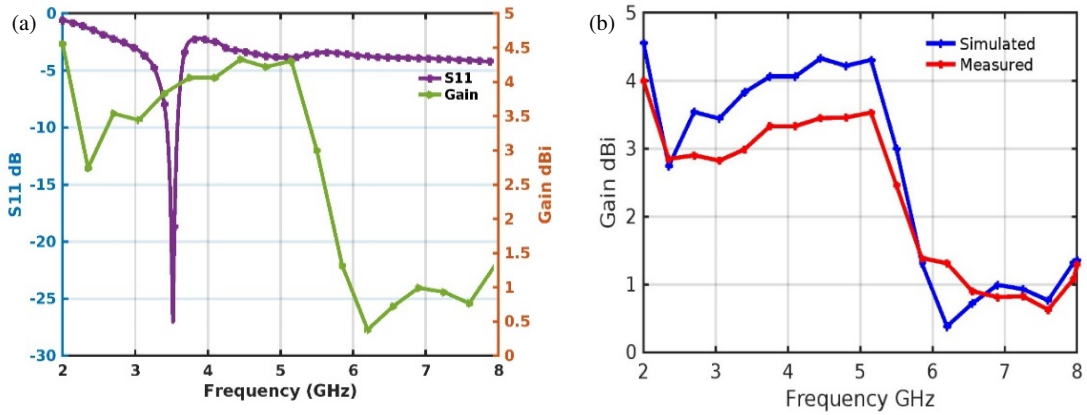

FIGURE 8. (a) S_{11} and gain of NCP-4 antenna. (b) Simulated gain vs measured one.

3. RESULTS AND DISCUSSION OF NCP ANTENNA

The proposed NCP-4 MIMO antenna was fabricated on an FR-4 substrate and experimentally validated using a vector network analyzer and a full anechoic chamber. S-parameter measurements were performed after full two-port short-open-load-through (SOLT) calibration at the SMA connector reference planes to eliminate cable and connector effects. During the measurements, the unused port was terminated with a 50 Ω matched load to emulate a practical MIMO operation.

The radiation characteristics were measured in a fully anechoic chamber using a standard gain horn antenna as a reference. The antenna under test was mounted on a low-dielectric foam support to minimize scattering, and measurements were conducted in the far-field region at 3.5 GHz to ensure an accurate gain and pattern characterization. Our analysis revealed several noteworthy observations in the design process, all of which are stated below. Figure 6 shows the NCP-4 antenna; (a) shows the front and back views of the fabricated NCP antenna; (b) explains the testing of the NCP-4 antenna using Vector Network Analyzer (VNA); and (c) NCP-4 in an anechoic chamber for testing. The simulated and measured NCP-4 antennas are compared, and their complete analysis is discussed.

The S_{11} results indicate that the measured performance closely aligns with the simulated performance, with S_{11} plots reaching −27 dB. Notably, the design exhibits excellent isolation, consistently exceeding −30 dB in both simulation and measurement, as depicted in Figure 7. The NCP-4 antenna S_{11} and gain are also plotted, and the antenna performance with two elements enhancing the gain to 4 dBi in the simulation is shown in Figure 8(a). Figure 8(b) shows a plot of the gain simulated and measured results with 4 and 3.04 dBi.

The E-field and H-field patterns are analyzed at a resonant frequency of 3.5 GHz and shown in Figure 9. To comprehensively evaluate the MIMO performance of the proposed NCP-4 antenna, the key diversity and multi-port parameters, namely the ECC, diversity gain (DG), mean effective gain (MEG), and total active reflection coefficient (TARC), are analyzed using well-established far-field and scattering parameter-based formulations [8].

ECC quantifies the correlation between the radiation patterns of antenna elements and is a critical indicator of the diversity performance in multi-path environments [4, 6]. In this study, ECC is calculated using the far-field radiation patterns, as expressed in (3), where $E_1(\theta, \phi)$ and $E_2(\theta, \phi)$ represent the complex radiated fields of the two antenna elements when the alternate port is terminated, and Ω is the solid angle. As shown in Figure 10, the proposed antenna exhibits a maximum ECC of 0.016 at 3.5 GHz, which is well below the acceptable limit

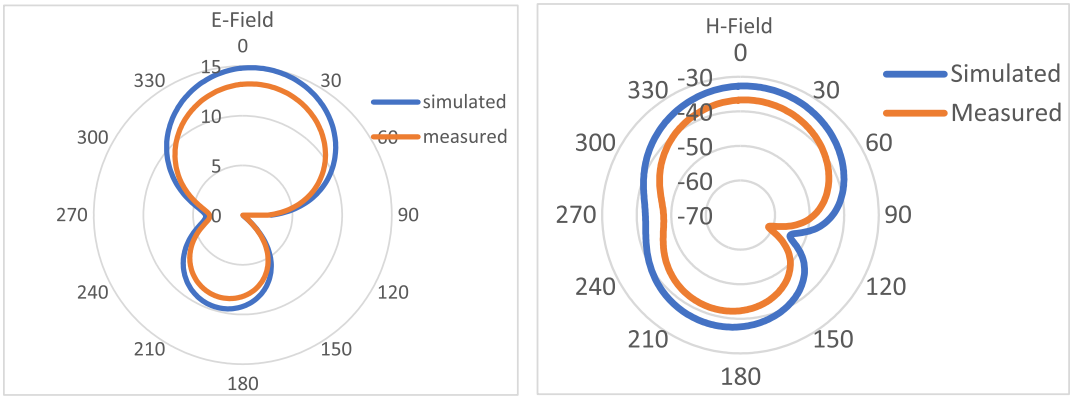

FIGURE 9. Simulated and measured E & H field patterns.

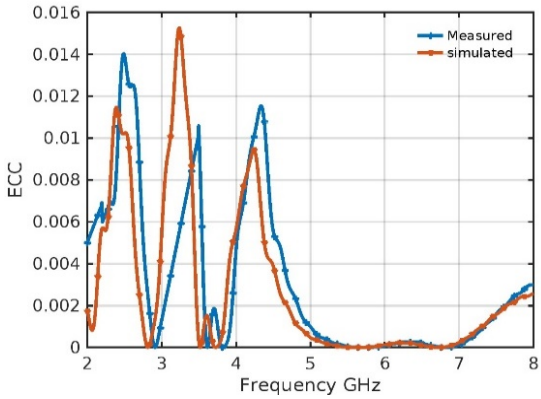

FIGURE 10. ECC vs frequency plot.

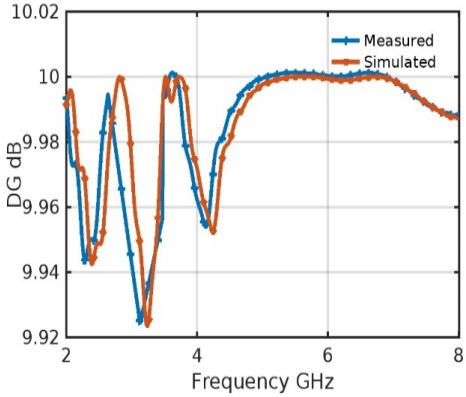

FIGURE 11. Diversity gain of proposed antenna.

of 0.5, confirming excellent pattern diversity. This low ECC is primarily attributed to the reduced ground plane and suspended diamond-shaped slots, which effectively redistribute the surface currents and minimize the pattern overlap between the elements.

The diversity gain (DG) derived from ECC using Equation (4) represents the improvement in signal reliability achieved through spatial diversity [8]. Figure 11 illustrates that the DG approaches 10 dB at the resonant frequency, indicating a near-ideal diversity performance. The achieved DG is a direct consequence of the high isolation and low field correlation ensured by the optimized inter-element spacing and symmetrical patch geometry.

$$\mathrm{ECC} = \frac{\left|\iint_{4\pi}\left[E_1(\theta,\emptyset) * E_2(\theta,\emptyset)\right] d\Omega\right|^2}{\iint_{4\pi}\left|E_1(\theta,\emptyset)\right|^2 d\Omega * \iint_{4\pi}\left|E_2(\theta,\emptyset)\right|^2 d\Omega} \quad (3)$$

$$\mathrm{DG} = \sqrt{1-\left|\rho_c\right|^2} \quad (4)$$

In addition, the mean effective gain (MEG) is evaluated to assess the average power received at each antenna element in a multi-path propagation environment [10]. MEG is computed using (5) based on the scattering parameters. As depicted in Figure 12, both antenna elements exhibit nearly identical MEG values, confirming balanced power reception and uniform radiation behavior. This balance results from the structural symmetry of the circular patch and identical slot configurations, which ensure equal excitation and radiation efficiency across the elements.

Furthermore, the total active reflection coefficient is analyzed to characterize the active impedance matching of the antenna when multiple ports are simultaneously excited [12]. TARC, calculated using (6), accounts for mutual coupling effects that are not captured by conventional S_{11} analysis. Figure 13 shows that the TARC remains below -10 dB across the operating band, validating effective impedance matching and stable radiation performance under multi-port excitation. The reduced ground plane and controlled current paths introduced by the circular cuts significantly suppress reflected power during simultaneous port operation.

$$\mathrm{MEG}_i = 0.5\left(1-\sum_{j=1}^{k}\left|S_{ij}\right|^2\right) \quad (5)$$

$$\mathrm{TARC} = \sqrt{\frac{\left|S_{11}+S_{12}\right|^2+\left|S_{21}+S_{22}\right|^2}{2}} \quad (6)$$

Overall, careful geometric tailoring of the NCP-4 patch, slots, and ground plane plays a crucial role in optimizing ECC, DG, MEG, and TARC, making it a strong candidate for compact sub-6 GHz (n78 band) 5G wireless applications.

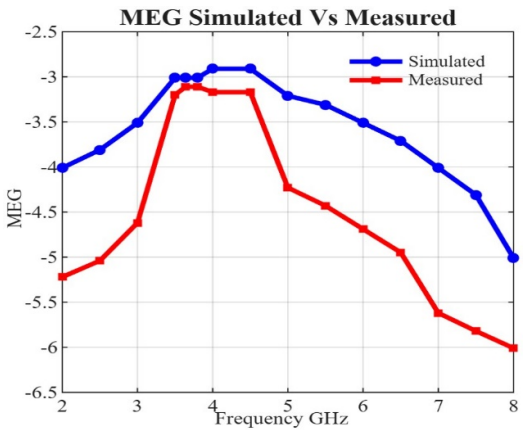

FIGURE 12. MEG of proposed antenna.

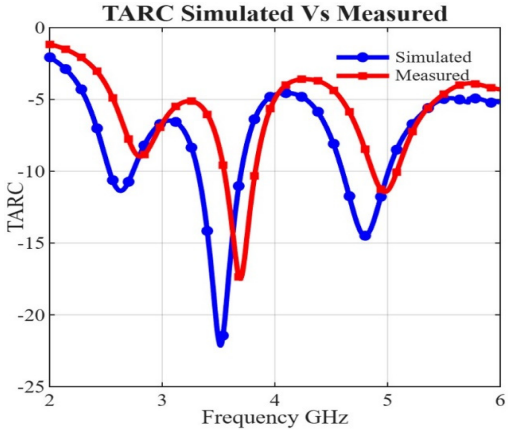

FIGURE 13. TARC of proposed antenna.

TABLE 2. Comparison with existing MIMO antenna designs.

Paper	Technique	Frequency GHz	Dimensions mm	Gain dBi	S_{11} dB	S_{21} dB
[1]	Decoupling cavity	4.2	168×168	7.9	-20	-24
[2]	Ceramic superstrate-based decoupling	3.5	100×100	1.5	-22	-25
[5]	Split Ring Resonator	5.7	79×55	3	-24	-25
[9]	Co-polarization	2.45	180×180	-	-20	-30
[10]	DGS	3.5	150×75	2.8	-23	-20
[11]	Patch is inter connected ground plane	2.7–4.94	60×55	2	-14	-27
[15]	Ground etching	3.5	150×75	4.2	-20	-22
[16]	Planar decoupling structure with metal	3.1–10.6	93×93	-	-31	-31
[17]	EBG metamaterial structure	2–7.5	100×41	1.6	-21	-30
[18]	Quasi-self-complementary	3–12	55×60	-	-24	-20
[19]	Planar monopole antenna	3.55	100×100	-	-18	-20
[20]	DGS	2.6	50×100	2.4	-20	-17
[21]	Polarisation diversity	2 to 6	70×70	1.5	-30	-20
[22]	Null points of E-field to decouple	3.5	85×50	3.3	-20	-20
[23]	Parasitic stubs	4.5	50×30	-	-28	-28
[24]	Metasurface based absorber	4 to 5.4	100×50	-	-11	-15
[25]	shared radiator antenna pair	3.3 to 5	100×50	-	-10	-17.5
NCP antenna	Interelement spacing and reduced ground	3.5	60×36	4	-27	< -30

4. COMPARISON

The proposed NCP-4 MIMO antenna is systematically evaluated against previously reported sub-6 GHz 5G antenna designs, as summarized in Table 2. Unlike many existing approaches that rely on additional decoupling structures or complex electromagnetic manipulation, the novelty of the proposed design lies in the combined use of a notched circular patch with suspended diamond-shaped slots and a reduced ground plane, achieving high isolation through intrinsic current redistribution rather than external decoupling elements.

Several reported designs employ auxiliary decoupling mechanisms that increase structural or fabrication complexity. For instance, the decoupling cavity-based antenna in [1] and the ceramic superstrate-assisted design in [2] achieve isolation levels of -24 dB and -25 dB, respectively, but at the expense of large footprints and the use of high-cost substrates. Similarly, metamaterial-based approaches [5, 17] and absorber-based techniques [24] improve isolation but require additional resonant elements, multi-layer alignment, or precise periodic structures, which increase manufacturing sensitivity and cost.

Ground-plane modification techniques, such as defected ground structure (DGS) and ground etching [10, 11, 15, 20], demonstrate moderate isolation enhancement; however, these methods often require extensive ground perturbation or larger antenna dimensions, which may adversely affect radiation stability and mechanical robustness. Planar decoupling and self-complementary structures [16, 18], while capable of wideband or high isolation performance, introduce intricate geometries and wide operational bandwidths that are not always necessary for narrowband 5G n78 applications.

In contrast, the proposed NCP-4 antenna achieves better isolation than −30 dB using only inter-element spacing optimization and a reduced ground plane, without employing vias, parasitic elements, electromagnetic band gaps (EBGs), metasurfaces, or multi-layer superstrates. This makes the design structurally simple, single-layer, and compatible with standard printed circuit board (PCB) fabrication. Furthermore, the antenna occupies a compact footprint of $60 \times 36\,\text{mm}^2$, which is significantly smaller than most reported designs operating at similar frequencies while still maintaining competitive gain and stable radiation characteristics.

The primary trade-off of the proposed antenna is its narrow impedance bandwidth, which limits its operation to a single 3.5 GHz 5G band. However, this narrowband behavior is acceptable for targeted n78 applications and contributes to improved isolation and radiation stability. Compared to array-based [9] or polarization-diverse [21] solutions, the proposed two-element configuration offers a balanced compromise among isolation performance, size reduction, and fabrication simplicity.

Overall, the comparison demonstrates that the proposed NCP-4 antenna provides a favorable combination of compact size, high isolation, and low design complexity, making it a practical and manufacturable solution for sub-6 GHz 5G MIMO systems.

5. CONCLUSION

A compact two-element notched circular patch MIMO antenna for sub-6 GHz 5G applications has been presented. The proposed design employs vertically positioned circular slots and suspended diamond-shaped slots on a reduced ground plane to effectively suppress surface current coupling between antenna elements. This simple structural modification enables high isolation ($S_{12} < -30\,\text{dB}$) at 3.5 GHz without increasing antenna size or using complex decoupling networks. The antenna achieves stable impedance matching with an S_{11} of −27 dB, acceptable gain, and excellent MIMO diversity characteristics, including low ECC (≤ 0.015) and high diversity gain ($\geq 9.98\,\text{dB}$), validating its suitability for compact 5G terminals. However, the antenna exhibits a narrow impedance bandwidth of approximately 140 MHz, which confines the operation to a single 5G band. The high isolation and a simple mechanism make the proposed antenna a promising design for scalable sub-6 GHz 5G and beyond wireless systems.

REFERENCES

[1] Luo, S., G. F. Pedersen, and S. Zhang, "Massive MIMO array design with high isolation by using decoupling cavity," *IEEE Transactions on Circuits and Systems II: Express Briefs*, Vol. 70, No. 3, 974–978, Mar. 2023.

[2] Liu, F., J. Guo, L. Zhao, G.-L. Huang, Y. Li, and Y. Yin, "Ceramic superstrate-based decoupling method for two closely packed antennas with cross-polarization suppression," *IEEE Transactions on Antennas and Propagation*, Vol. 69, No. 3, 1751–1756, Mar. 2021.

[3] Tran, H. H. and N. Nguyen-Trong, "Performance enhancement of MIMO patch antenna using parasitic elements," *IEEE Access*, Vol. 9, 30 011–30 016, 2021.

[4] Wen, D., Y. Hao, H. Wang, and H. Zhou, "Design of a MIMO antenna with high isolation for smartwatch applications using the theory of characteristic modes," *IEEE Transactions on Antennas and Propagation*, Vol. 67, No. 3, 1437–1447, Mar. 2019.

[5] Luo, S., Y. Li, Y. Xia, and L. Zhang, "A low mutual coupling antenna array with gain enhancement using metamaterial loading and neutralization line structure," *Applied Computational Electromagnetics Society Journal (ACES)*, Vol. 34, No. 3, 411–418, 2019.

[6] Li, J., X. Zhang, Z. Wang, X. Chen, J. Chen, Y. Li, and A. Zhang, "Dual-band eight-antenna array design for MIMO applications in 5G mobile terminals," *IEEE Access*, Vol. 7, 71 636–71 644, 2019.

[7] Aw, M. S., K. Ashwath, T. Ali, *et al.*, "A compact two element MIMO antenna with improved isolation for wireless applications," *Journal of Instrumentation*, Vol. 14, No. 6, P06014, Jun. 2019.

[8] Chouhan, S., D. K. Panda, and V. S. Kushwah, "Modified circular common element four-port multiple-input-multiple-output antenna using diagonal parasitic element," *International Journal of RF and Microwave Computer-Aided Engineering*, Vol. 29, No. 2, e21527, 2019.

[9] Zhang, Y.-M., S. Zhang, J.-L. Li, and G. F. Pedersen, "A transmission-line-based decoupling method for MIMO antenna arrays," *IEEE Transactions on Antennas and Propagation*, Vol. 67, No. 5, 3117–3131, May 2019.

[10] Li, M.-Y., Y.-L. Ban, Z.-Q. Xu, J. Guo, and Z.-F. Yu, "Tri-polarized 12-antenna MIMO array for future 5G smartphone applications," *IEEE Access*, Vol. 6, 6160–6170, Dec. 2017.

[11] Sarkar, D. and K. V. Srivastava, "A compact four-element MIMO/diversity antenna with enhanced bandwidth," *IEEE Antennas and Wireless Propagation Letters*, Vol. 16, 2469–2472, 2017.

[12] Gali, R. L. and M. Tatineni, "Design of a dual-band H-cut circular antenna with various decoupling methods for 5G NR band," in *2025 International Conference on Inventive Computation Technologies (ICICT)*, 1935–1939, Kirtipur, Nepal, Apr. 2025.

[13] Talha, M. Y., K. J. Babu, and R. W. Aldhaheri, "Design of a compact MIMO antenna system with reduced mutual coupling," *International Journal of Microwave and Wireless Technologies*, Vol. 8, No. 1, 117–124, Feb. 2016.

[14] Anitha, R., P. V. Vinesh, K. C. Prakash, P. Mohanan, and K. Vasudevan, "A compact quad element slotted ground wideband antenna for MIMO applications," *IEEE Transactions on Antennas and Propagation*, Vol. 64, No. 10, 4550–4553, Oct. 2016.

[15] Wong, K.-L., J.-Y. Lu, L.-Y. Chen, W.-Y. Li, and Y.-L. Ban, "8-antenna and 16-antenna arrays using the quad-antenna linear array as a building block for the 3.5-GHz LTE MIMO operation in the smartphone," *Microwave and Optical Technology Letters*, Vol. 58, No. 1, 174–181, Jan. 2016.

[16] Radhi, A. H., R. Nilavalan, Y. Wang, H. S. Al-Raweshidy, A. A. Eltokhy, and N. A. Aziz, "Mutual coupling reduction with a wideband planar decoupling structure for UWB-MIMO antennas," *International Journal of Microwave and Wireless Technologies*, Vol. 10, No. 10, 1143–1154, Jul. 2018.

[17] Alsultan, R. G. S. and G. O. Yetkin, "Mutual coupling reduction of E-shaped MIMO antenna with matrix of C-shaped resonators," *International Journal of Antennas and Propagation*, Vol. 2018, No. 1, 4814176, Feb. 2018.

[18] Sharawi, M. S., A. B. Numan, M. U. Khan, and D. N. Aloi, "A dual-element dual-band MIMO antenna system with enhanced

isolation for mobile terminals," *IEEE Antennas and Wireless Propagation Letters*, Vol. 11, 1006–1009, Aug. 2012.

[19] Zhao, X., S. P. Yeo, and L. C. Ong, "Decoupling of inverted-F antennas with high-order modes of ground plane for 5G mobile MIMO platform," *IEEE Transactions on Antennas and Propagation*, Vol. 66, No. 9, 4485–4495, Sep. 2018.

[20] Zhu, J., S. Li, B. Feng, L. Deng, and S. Yin, "Compact dual-polarized UWB quasi-self-complementary MIMO/diversity antenna with band-rejection capability," *IEEE Antennas and Wireless Propagation Letters*, Vol. 15, 905–908, Sep. 2015.

[21] Saad, A. A. R., "Approach for improving inter-element isolation of orthogonally polarised MIMO slot antenna over ultra-wide bandwidth," *Electronics Letters*, Vol. 54, No. 18, 1062–1064, Sep. 2018.

[22] Shehata, M., M. S. Said, and H. Mostafa, "Dual notched band quad-element MIMO antenna with multitone interference suppression for IR-UWB wireless applications," *IEEE Transactions on Antennas and Propagation*, Vol. 66, No. 11, 5737–5746, 2018.

[23] Hasan, M. M., M. T. Islam, T. Alam, A. Alzamil, and M. S. Soliman, "Electromagnetic coupling shielding in compact MIMO antenna using symmetric T-shaped metamaterial structure for 5G communications," *Optics & Laser Technology*, Vol. 169, 110046, 2024.

[24] Puri, V. and H. S. Singh, "Design of an isolation improved MIMO antenna using metasurface based absorber for wireless applications," *Optik*, Vol. 259, 168963, 2022.

[25] Zeng, W.-F. and F.-C. Chen, "Wideband high-isolation antenna pair for 5G smartphones using multiple characteristic modes," *AEU — International Journal of Electronics and Communications*, Vol. 170, 154856, 2023.